Turkish Journal of Earth Sciences

Volume 30 | Number 3 Article 4

1-1-2021

Luminescence dating of Quaternary marine terraces from the coastal part of Eastern Black Sea and their tectonic implications for the Eastern Pontides, Turkey

MUSTAFA SOFTA

JOEL QG SPENCER

HASAN SÖZBİLİR

SEBASTIEN HUOT

TAHİR EMRE

TÜBİTAK

Turkish Journal of Earth Sciences

http://journals.tubitak.gov.tr/earth/

Research Article

Turkish J Earth Sci
(2021) 30: 359-378

doi:10.3906/yer-2005-21

Luminescence dating of Quaternary marine terraces from the coastal part of Eastern Black Sea and their tectonic implications for the Eastern Pontides, Turkey

Mustafa SOFTA[1, 2], Joel Q. G. SPENCER[2], Hasan SÖZBİLİR[1], Sebastien HUOT[3], Tahir EMRE[1]

[1]Department of Geology, Dokuz Eylül University, İzmir, Turkey

[2]Department of Geology, Kansas State University, Manhattan, KS, USA

[3]Illinois State Geological Survey, University of Illinois at Urbana-Champaign, Champaign, IL, USA

Received: 18.05.2020 • **Accepted/Published Online:** 03.01.2021 • **Final Version:** 17.05.2021

Abstract: The timing of the deposition of the well-preserved Quaternary marine terraces in the coastal region of northeastern Turkey are crucial in understanding the Quaternary tectonics of the Pontides. The chronology of raised marine terraces between Trabzon and Rize has remained unrevealed because of chronologic limitations. This study aims to establish chronology for the terrace deposits by applying optically stimulated luminescence (OSL) dating methods using single aliquot regenerative dose (SAR) techniques on quartz grains extracted from marine terraces. Eleven samples were collected from the lowest three Quaternary marine terraces. The OSL ages clusters into three groups: 52.4 ± 4.6 to 60.0 ± 4.7 ka (terrace level T1); 16.8 ± 0.8 to 33.9 ± 2.8 ka (T2); and 11.7 ± 0.9 ka (T3). This chronology is consistent with the classical terrace stratigraphy; i.e. younger terraces are located at lower elevations and vice versa for the older terraces. We correlate the established terrace chronology with MIS 3c, MIS 3a, and MIS 1. We calculated apparent uplift rates are 0.98 ± 0.12 mm/year, 1.39 ± 0.26 mm/year, and 1.50 ± 0.78 mm/year from marine terrace levels 1, 2, and 3, respectively. Based on the existing eustatic sea-level data/curve, we estimated tectonic uplift rates up to 5 mm per year. Our results indicate that the coastal region of the Eastern Pontides experienced three accumulation periods, with sea-level highstands overprinting the uplifting coastline, and the coastal region of Eastern Pontides has been tectonically active from Late Pleistocene to Early Holocene. This study reveals that marine terraces in the coastal region of northeastern Anatolia might have displaced by the South Black Sea Fault which ultimately points to a regional subsidence with the higher uplift rate, and it points to a differential uplift along the Eastern Pontides.

Key words: Optically stimulated luminescence (OSL) dating, Late Quaternary marine terraces, uplift rate, Black Sea, Eastern Pontides

1. Introduction

The chronology of the marine terraces is linked to their time of deposition and a critical component in the understanding of Quaternary tectonism worldwide. Stratigraphic associations and geographic distributions of marine deposits, when combined with the chronology, can provide beneficial knowledge regarding global and regional tectonic movements, as well as sea-level changes. Various Quaternary geochronological techniques have been used to establish the age of these sequences to enable comparison to global climatic and tectonic pattern changes in many regions (e.g., Yaltırak et al., 2002; Pedoja et al., 2006, 2018; Tarı et al., 2018; Özalp, 2020), but each method has its advantages, disadvantages, and limitations, such as bedrock geology, age construction, absence of suitable material. However, radiocarbon dating (^{14}C) is the most used technique for terrace chronologies, but ^{14}C dates, which constrain the chronology of the Late Pleistocene-Holocene deposits are rare because of the absence of organic material in these deposits as well as the range of the radiocarbon dating [max. 60 ka, Beukens (1994)]. Other dating techniques such as U/Th (e.g., Schwarcz, 1989), OSL (e.g., Aitken, 1985), ESR (e.g., Grün, 1989) and cosmogenic nuclides (e.g., Sançar et al., 2020) have also been applied to reconstruct terrace chronologies. In recent years, optically stimulated luminescence (OSL) dating has become a widely used and well-known dating technique (e.g., Preusser et al., 2008; Rhodes, 2011). In particular, OSL dating has been successfully applied to marine terrace deposits (e.g., Tanaka et al., 1997; Choi et al., 2003a, 2003b; Rhodes et al., 2006; Jacobs, 2008; Gurrola et al., 2014; Bateman, 2015; Lamothe, 2016).

Marine deposits at various elevations on the coastal region of Eastern Pontides have been studied since the mid-1800's (Hamilton, 1842; Oswald, 1906; Karajiyan, 1920; Ardel, 1943; Erol, 1952; Semerci, 1990; Solmaz,

* Correspondence: mustafa.softa@deu.edu.tr

1990; Yilmaz et al., 1998; 2005; Keskin, 2007; Keskin et al., 2011; Aytac, 2012; Yildirim et al., 2013). The emerged marine terraces are located on the coastal region of Eastern Pontides, on the push-up system linked with the Black Sea Fault and the Borjomi-Kazbegi Fault (Softa et al., 2018, 2019). The emerged paleoshorelines are notable, rising in altitude from three meters to over one hundred meters above sea-level in the study area. The coastal region of Pontides is used to decipher geologic and geomorphologic indications of significant regional tectonic activity and Quaternary sea-level changes (e.g., Yaltırak, 2002; Erginal et al., 2013; Yildirim et al., 2011, 2013).

Recently, the chronology of the marine deposits in the western Pontides was reconstructed with OSL (e.g., Yaltırak, 2002; Yildirim et al., 2013). However, the studies focusing on the understanding the timing, rate and pattern Quaternary deformation in the Eastern Pontides are rare except for Keskin (2007) and Keskin et al. (2011). These studies applied electron spin resonance (ESR) techniques to date gastropod and bivalve macrofossils collected from the four lowest terraces, which were dated 408.0 ± 67.5 ka (T3), 292.5 ± 49.8 ka (T2), 124.8 ± 26.0 ka (T1), and 5.1 ± 0.3 ka (TH) in Trabzon. To bridge the gap in the chronology of these terraces, we aimed at a better understanding of the interaction with active tectonics, climate, and the Quaternary uplift in the Eastern Pontides by mapping terraces and faults, and at exploring the competence of OSL dating by using quartz grains extracted from terrace deposits. This study marks the first OSL dating using the single aliquot regenerative dose (SAR) protocol (Murray and Wintle, 2000, 2003; Wintle and Murray, 2006) applied to marine terraces in the coastal area of Eastern Pontides between Trabzon and Rize, including the Keskin et al.'s (2011) outcrops in Trabzon. In brief, our OSL chronology supports the description of the building of marine terraces and various tectonic movements, as well as sea-level fluctuations in this area. This information provides better understanding of tectonism linked with the rapid vertical uplift of Eastern Pontides.

1.1. Late Pleistocene-Holocene sea-level changes of the Black Sea

The Black sea is one of the largest semienclosed sea in the world, and it is connected to global oceans via the Bosphorus strait. During the Quaternary, this connection was cut off and reconnected periodically because the global sea-level dropped below the Bosphorus straits during glacial periods and sea-level rise during the transition interglacial periods (e.g., Smith et al., 1995; Aksu et al., 20002; Çağatay et al., 2015). According to Badertscher et al. (2011), these transition periods repeated several times during the past 670 ka. One of the important consequences of these cut-off and connection events is the migration of marine organisms into the Black Sea. For example, during the MIS 1 and MIS 3, saline Mediterranean water penetrated to Black Sea via Dardanelles and Bosphorus straits (e.g., Aksu et al., 2002; Yaltırak et al., 2002). Especially, marine conditions during the MIS 3a and 3c interglacials were suitable for macro and micro marine organisms in the Black Sea (e.g., Aksu et al., 2002; Yaltırak et al., 2002). In the literature, while there is a consensus for saline water and fresh-melted water exchange event during the MIS 1 and Late MIS 2, the MIS 3 to MIS 7 events might seem to be controversial due to the unrevealed archives of these events and their chronology (e.g., Aksu et al., 2002; Hiscott et al., 2002, 2007; Ryan, 2007).

2. Study area

2.1. Geological background and neotectonic setting

The Pontides is divided tectonically into three zones, namely, the Western, Central and Eastern Pontides due to their different geologic and tectonic features (e.g., Yılmaz et al., 1997). Extending ~500 km by ~200 km, the Eastern Pontides orogenic belt lies along the southeastern coast of the Black Sea basin. The latter is divided into two parts, the western and eastern Black Sea basins, separated by the Andrusov high (Figure 1a).

Numerous studies have been proposed to shed light on the geologic and geodynamic evolution of the Eastern Pontides (e.g., Dewey et al., 1973; Adamia et al., 1977; Şengör and Yılmaz, 1981; Ustaömer and Robertson, 1996; Bektaş at al., 1999; Eyuboglu et al., 2006, 2007, 2011). According to these studies, the Eastern Pontides is accommodated by progressive deformation between the North Anatolian Fault (NAF) and the Black Sea within the Eastern Black Sea Mountain Belt (Figure 1a). It is on a transpressional deformation zone due to the N-NW direction of the Arabian Plate which is considered to cause uplift and crustal thickening in the Pontides.

The Eastern Pontides is divided tectonically into northern, southern and axial subzones by many researchers (e.g., Özsayar, 1971; Bektaş et al., 1995; Eyuboglu et al., 2006, 2007). The boundaries of each zone are represented by NE-SW, E-W, and NW-SE trending fault zones, which play a significant role in the active tectonics of the Eastern Pontides (Figure 1b).

In the Eastern Pontides between the Black Sea and the NAF, there are several active and potentially active faults (Softa et al., 2018, 2019) (Figure 1b). There, the NAF has multiple riedel faults, such as the Northeast Anatolian Fault (NEAF) (Badgley, 1965; Riedel, 1929; Vialon et al., 1976; Wilcox et al., 1973). The NEAF is about 800 km long, and northeast trending dextral strike-slip fault connected with a north-dipping thrust fault around the Bayburt city namely Borjomi-Kazbegi Fault (BKF) that is about 250

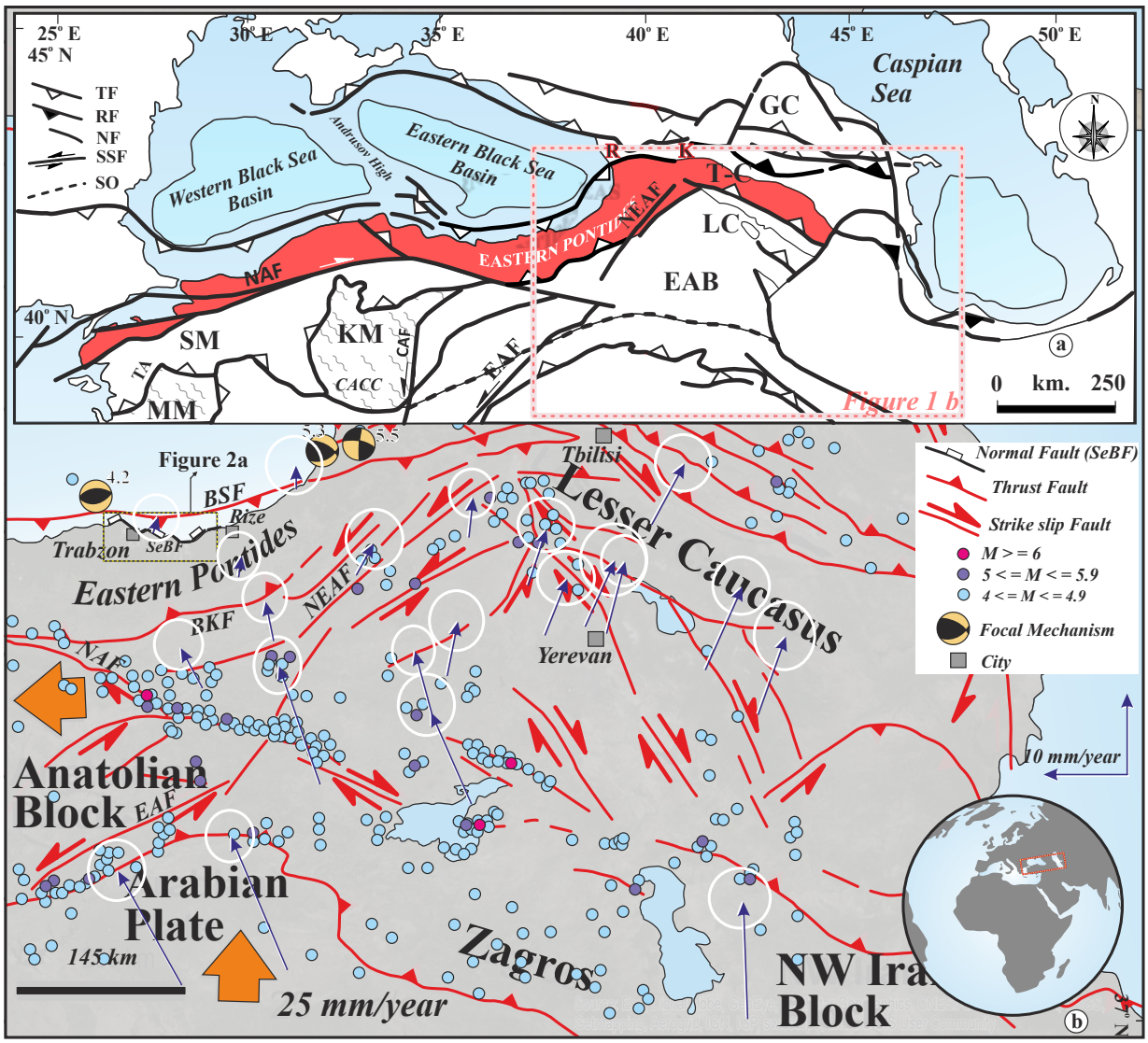

Figure 1. a) Main geologic and tectonic map of the Anatolia-Caucasus region, after Sosson et al. (2016), and Hässig et al. (2016) with modifications. NAF: North Anatolian Fault, CAF: Central Anatolian Fault, EAF: East Anatolian Fault, GC: Greater Caucasus, LC: Lesser Caucasus, T-C: Trans Caucasus, KM: Kırşehir Massif, MM: Menderes Massif, SM: Sakarya Massif, CACC: Central Anatolian Crystalline Complex, EAB: East Anatolian Block, R-K: Rioni Kura Basin, TF: Thrust Fault, RF: Reverse Fault, NF: Normal Fault, SSF: Strike Slip Fault, SO: Suspected Ophiolite. b) Simplified neotectonic map of the Eastern Pontides and the nearest region (modified from Tsereteli et al., 2016; Avagyan et al., 2010 and TPAO[1]). GPS velocities are compiled from McClusky et al. (2000), (2003) and Nilforoushan et al. (2003). BSF: Black Sea Fault, BKF: Borjomi Kazbegi Fault, SeBF: Southeast Blacksea Fault.

[1]TPAO (2010). Turkish Petroleum Oil Company (TPAO) (2010). Seismic sections [online]. Website http://www.tpao.gov.tr [accessed 10 August 2010].

km length (Westaway, 1994; Koçyiğit et al., 2001; Softa et al., 2018, 2019). Besides, the NEAF and NAF is connected by a 400 km long northeast trending and south dipping Black Sea Fault (BSF) that has a ramp-flat structure. The Eastern Pontides continues to uplift gradually at a rate of more than 0.5 mm per year because of this strain, progressed by the push-up geometry with the thrust faults of BSF at sea and the BKF on the land (Softa et al., 2018, 2019). In addition to these transpressional system, which are accommodated by the uplift in the Eastern Pontides, there are dip/oblique-slip normal fault segments of an en-echelon geometry known as Southeast Black Sea Fault that is composed of 65-km long and more than 1 km wide en-echelon distributed fault zone (Softa et al., 2019).

2.2. Stratigraphy

The lithostratigraphy of the study area consists of seven units: (I) Çağlayan Formation, (II) Çayırbağ Formation, (III) Bakırköy Formation, (IV) Kabaköy Formation, (V) Kaymaklı Formation, (VI) Beşirli Formation, (V) red clays, (VI) alluvium and (VII) marine terraces (Figure 2). The oldest unit in the study area is the Late Cretaceous (Campanian-Maastrichtian)-Paleogene units, characterized by volcano-sedimentary rocks and divided into the Çağlayan, Çayırbağ, and Bakırköy Formations (Gedikoğlu, 1970; Güven, 1993). The unconformably overlying Eocene Kabaköy Formation is composed of basalt, andesite with pyroclastic fragments, some sandstone and limestone with nummulites. The Kaymaklı Formation contains Miocene clayey and sandy siltstone; this unit was originally named Pontian clays by Özsayar (1971) and overlies the unconformably the older units. The Beşirli Formation is represented by Pliocene andesitic and basaltic agglomerate, coarse-grained sandstone, tuff, and claystone-marl-sandstone intercalations, and this unit is seen close to the seashore. Red clays are locally composed of red colored silt, mud and clays with nearly horizontal layers. Quaternary alluvium and marine terraces unconformably overlie the Beşirli Formation and the Kabaköy Formation (e.g., Yilmaz et al., 1998) (Figure 2c).

Here, we focus on the youngest unit, the Quaternary alluvium, and terraces, which are mostly observed on hanging walls and footwalls of the normal faults (Figures 2b and 2c). For in-depth review and discussions about the older units, we recommend readers examine the following resources (e.g., Gedikoğlu, 1970; Özsayar, 1971; Güven, 1993; Eyuboglu et al., 2006).

3. Methodology

The methodology is given in three sections. In the first section, we present: (i) exploring stratigraphy and mapping the faults and marine terraces in detail, and (ii) sampling

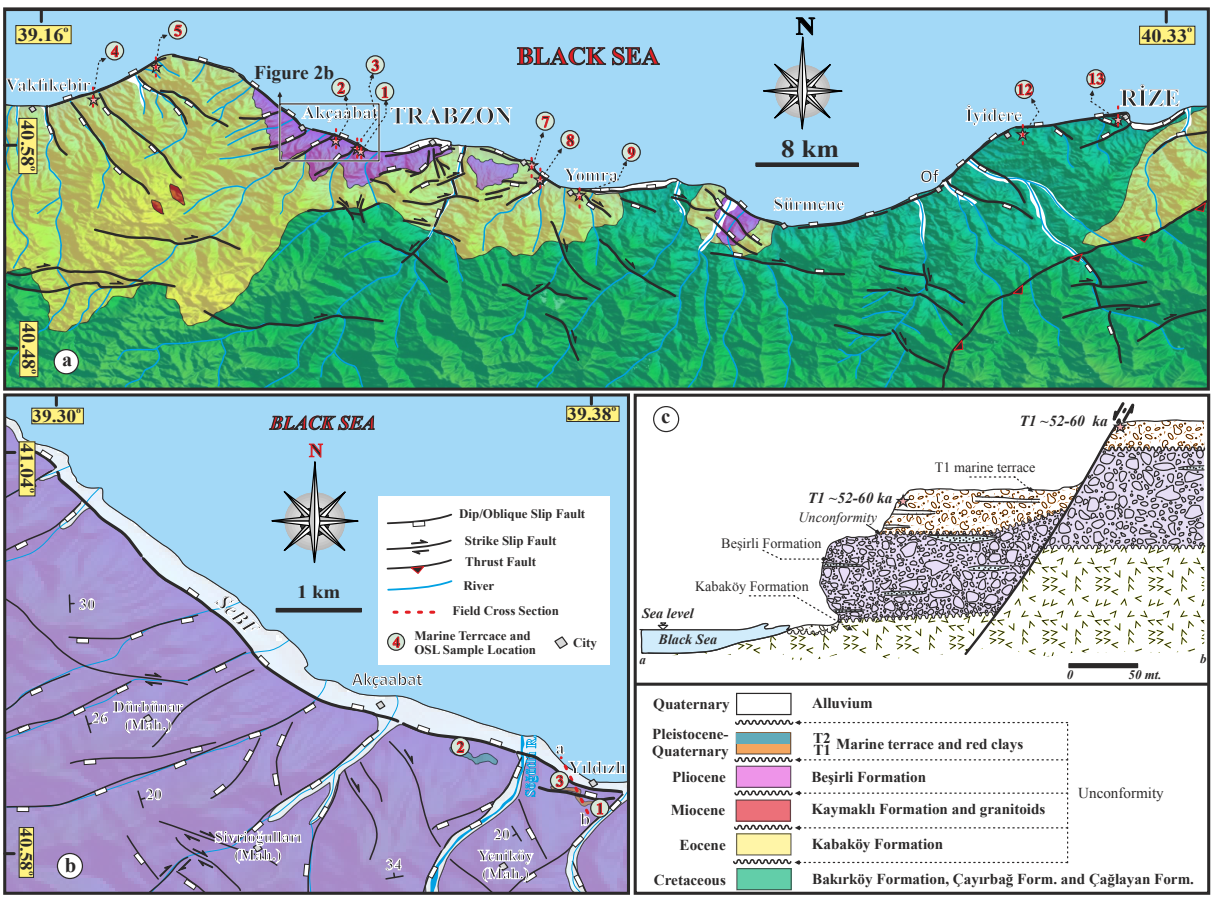

Figure 2. a) Geological map of the studied region, after Güven (1993) with modifications. Hillshade generated from SRTM-30m (Shuttle Radar Topography Mission)[1] b) Detailed geological map of the Trabzon-Akçaabat and nearest region, SeBF: Southeast Blacksea Fault. c) Field crosssection with geological relation of marine terraces has displaced by the Southeast Blacksea Fault.

[1]NASA (2021). Earth Science Data Systems [online]. Website http://earthdata.nasa.gov. [accessed 05 January 2020].

marine terraces for OSL dating. In the second section, we focus on laboratory process on luminescence dating, and in the third on the calculation of Quaternary uplift rate.

3.1. Fieldwork and sampling

The Eastern Pontides was first investigated with a combination of Google Earth images and the 30 m resolution SRTM maps and digitized 1/25,000 (version 1967) topographic maps from the General Command of Mapping (Turkey). We explored three marine terrace deposits. To obtain the altitudes, hand type global positional system [GPS ± 10 m (instrumental error of the GPS)] was used.

Optically Luminescence dating (OSL) is one of the state of arts and well-known technique to constrain the timing of identified layers worldwide (e.g., Fattahi et al., 2006; Preusser et al., 2008; Fattahi et al., 2010; Rhodes, 2011; Stahl et al., 2016; Tsodoulos et al., 2016). As each terrace level constituted materials of possibly different sea-level changes, making an ideal sampling location in order not to be affected possibly postdepositional contamination. Eleven samples were collected from three marine terraces using metal cylinders, taking care of limit any light exposure on the open cylinder ends and assuring that terrace sediments completely filled the cylinder to avoid mixing of light-exposed grains within the cylinder during the transport. As an additional precaution, sampling was undertaken during a moonless night. The following terraces are arranged stratigraphically from youngest to oldest (Table 1).

To define the depositional environment, micropaleontological sampling was implemented. A total of 11 samples were collected. The sample preparations include some routine washed techniques such sieving, drying, chemical process (hydrogen peroxide and acetic acid), and the subsampling for the analyses. Then all material was analyzed under an Olympus BX50 binocular microscope for microfossils and photomicrographs were taken by an Olympus E330 camera attached to the microscope.

3.2. Luminescence dating

3.2.1. Sample preparation

Mineral preparation and OSL measurements were carried out at the Luminescence Research and Dating Laboratory of the department of geology at Kansas State University. The preparation of quartz for OSL dating was similar to the standard procedures described by Aitken (1998) and Spencer and Robinson (2008), and the preparation steps were as follows. The first step involved removing the sample from the cylinder; to minimize the possibility of analyzing grains that were inadvertently bleached during or postsampling, approximately 3 cm of deposit was removed from the ends of each cylinder. Field moisture content was assessed for both the sediment removed from the cylinder ends and the material for dating in the central part of the cylinder. This was carried out by comparison of sediment mass before and after weight stabilization in a 50 °C oven. Saturated water content estimates were also recorded. The second process was wet sieving, and a grain size fraction of 125–180 μm was chosen for each sample. Silicate-rich grains were extracted from the samples after these processes using 10% HCl and 30% H_2O_2 for the removal of carbonates and organic matter, respectively;

Table 1. Sample details and data from gamma spectrometry.

Sample ID[a]		Altitude (m)	U (226Ra) (ppm)[b]		Th (ppm)		K (%)	
			<2mm	>2mm	<2mm	>2mm	<2mm	>2mm
TR-3	T1	60 ± 4	0.39 ± 0.03	0.99 ± 0.04	2.35 ± 0.06	4.32 ± 0.11	0.38 ± 0.02	1.79 ± 0.04
TR-1		48 ± 5	0.53 ± 0.03	1.10 ± 0.06	2.49 ± 0.09	4.35 ± 0.12	0.51 ± 0.02	1.27 ± 0.04
TR-7	T2	43 ± 2	3.06 ± 0.09	2.45 ± 0.09	11.16 ± 0.22	8.98 ± 0.26	1.24 ± 0.03	1.44 ± 0.05
TR-8		42 ± 2	3.92 ± 0.11	4.39 ± 0.13	10.86 ± 0.19	11.19 ± 0.27	1.43 ± 0.04	1.59 ± 0.05
TR-5		35 ± 3	1.06 ± 0.04	1.44 ± 0.05	4.72 ± 0.13	6.42 ± 0.51	1.73 ± 0.04	2.45 ± 0.05
TR-6		45 ± 5	0.77 ± 0.04	0.85 ± 0.04	3.82 ± 0.14	4.26 ± 0.13	1.08 ± 0.03	1.12 ± 0.03
TR-2		42 ± 4	1.25 ± 0.05	1.38 ± 0.06	5.50 ± 0.18	6.76 ± 0.17	1.49 ± 0.03	2.15 ± 0.06
TR-4		35 ± 3	0.76 ± 0.03	2.39 ± 0.08	3.50 ± 0.07	11.40 ± 0.27	0.79 ± 0.02	2.70 ± 0.06
TR-12		37 ± 2	3.19 ± 0.09	1.05 ± 0.05	8.25 ± 0.19	3.17 ± 0.19	1.30 ± 0.03	0.75 ± 0.03
TR-13		36 ± 2	1.85 ± 0.06	1.84 ± 0.06	6.92 ± 0.16	4.60 ± 0.11	2.16 ± 0.05	1.07 ± 0.03
TR-9	T3	27 ± 3	2.02 ± 0.06	1.66 ± 0.07	9.74 ± 0.18	6.83 ± 0.24	1.09 ± 0.03	1.57 ± 0.05

[a] See text for the sampling localities and sample details (Figures 2 and 4), and T1; T2; T3 indicates the terrace level.
[b] Radium-226 is a daughter product of the uranium-238 series.

next came density separation of heavy minerals (>2.70 g/cm^3) with lithium metatungstate (LMT) heavy liquid, and then we used 48% HF for 40 min to etch the outer surface of quartz grains affected by external alpha radiation and to eliminate feldspar grains. This was followed by another 10% HCl treatment to redissolve and remove any precipitated fluorides.

All samples were then washed with deionized water and acetone and then briefly oven dried at 50 °C. Prepared quartz aliquots of 1-mm, and in some cases 3-mm, diameter circles of grains were fixed to ~9.8-mm-diameter stainless steel discs using silicone oil and a spray template. All sample preparation including chemical processes and OSL measurement procedures was conducted under low intensity red safe lighting.

3.2.2. Equivalent dose (D_e) measurements

OSL analytical procedures followed the methodology outlined in Spencer and Robinson (2008) and Spencer et al. (2015). OSL measurements were carried out on a Risø TL/OSL Model DA-20 reader (Bøtter-Jensen et al., 2003) with blue-green (470 nm, FWHM 20 nm) and infrared (870 nm, FWHM 40 nm) light-emitting diode (LED) optical stimulation sources, with detection in the UV via an EMI 9235QB photomultiplier tube fitted with 7.5 mm of Hoya U-340 filter. Laboratory irradiations were implemented using a calibrated ^{90}Sr/^{90}Y beta source (~0.14 Gy s^{-1}) on the reader.

The D_e of all quartz aliquots was determined using a SAR protocol (Murray and Wintle, 2000, 2003; Wintle and Murray, 2006). OSL measurements comprised 40 s diode stimulation at a sample temperature of 125 °C. For calculation of sensitivity-corrected OSL signals and D_e estimates the OSL signal was defined as the initial 0.8 s integral with a background integral of the final 8 s (Wintle and Murray, 2000) (Figure 3a). The test dose administered for sensitivity correction was ~14 Gy. The D_e values were found using interpolation of the natural OSL signal with a best-fit saturating exponential function to the regenerative OSL data (Figure 3b).

To determine optimal preheat and cutheat treatments, dose recovery tests (Roberts et al., 1999; Murray and Wintle, 2003) were carried out with preheat variation (Spencer and Robinson, 2008). Dose recovery and D_e data were analyzed with typical acceptance thresholds of 10% for measured-to-given ratios and recycling ratios and 5% for recuperation levels (Murray and Wintle, 2000, 2003). Uncertainty in D_e was calculated from counting statistics, curve fitting errors, and instrumental uncertainty (Duller, 2007). Test results that exceeded thresholds were accepted with allowance for typical uncertainty limits. At the end of each SAR cycle, a hot bleach treatment of 40 s OSL at 280 °C (Murray and Wintle, 2003) was added. IR depletion tests (Duller, 2003) were used to confirm the absence of contaminant signals.

Dose-distribution analysis was implemented for all quartz aliquots. The D_e data were evaluated by means of a radial plot (Galbraith, 1990) together with sample-specific estimates of overdispersion (Galbraith et al., 2005). D_e data for each sample were analyzed using both the minimum age model (MAM) and the central age model (CAM) (Galbraith et al., 1999). All results were assessed together with geologic, geomorphologic, and sedimentological information from the study area.

3.2.3. Dose rate determination

Environmental dose-rates were assessed using high resolution gamma spectrometry measurements (Murray et al., 1987; Gilmore, 2008) conducted at the Illinois Geological Survey, and from calculations of the ionizing cosmic ray dose-rate component (Prescott and Hutton, 1994), (Table 1).

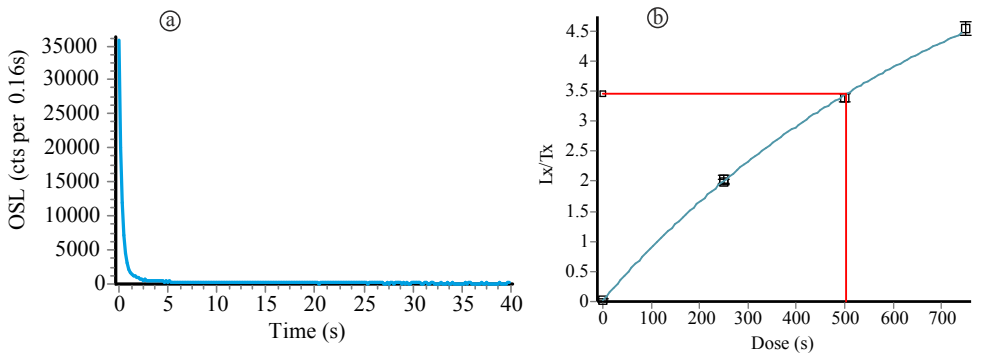

Figure 3. a) A typical OSL decay curve for a quartz aliquot of sample TR-8 showing the signal as measured with blue light emitting diodes. The x-axis is the time of measurement in seconds(s) and the y-axis is photon counts/0.16 s over the course of the 40 s measurement period. A sharp decay is seen indicating the fast component of the OSL signal. b) TR-8 growth curve (using a saturating exponential function), with the natural OSL plotted on the Lx/Tx axis at ~3.5. The x-axis is the dose indicated in seconds; interpolation of natural OSL gives D_e of ~70 Gy. The y-axis shows the sensitivity corrected (regenerative OSL response over the test dose OSL response) OSL.

Sediment in a number of the OSL samples was poorly sorted with some clasts exceeding ~1–2 cm in size. Normalized by weight, larger clasts are primarily a gamma emitter, as most of the beta particles, internally released via radioactive disintegrations, are reabsorbed within the clast (i.e. Urbanova et al., 2015). Because of this, we evaluated the uranium, thorium, and potassium content by distinguishing two separate size fractions of <2 mm and >2 mm in order to account for the effect on the gamma dose-rate from different clast sizes, for the first time. Material removed from the cylinder ends was dried, sieved into <2 mm and >2 mm fractions, and their mass recorded. The size fractions were crushed and mounted in thin cylindrical plastic boxes (about 20 g). Each was sealed with wax, stored for a minimum of 21 days to restore the postradon equilibrium, and then gamma spectrometry measurements conducted.

Dry beta dose-rate was calculated from the <2 mm fraction data; dry gamma dose-rate, $\dot{D}_{\gamma,total}$, was calculated as follows:

$$\dot{D}_{\gamma,total} = x\,\dot{D}_{\gamma,<2} + (1-x)\,\dot{D}_{\gamma,>2},$$

where $\dot{D}_{\gamma,<2}$ and $\dot{D}_{\gamma,>2}$ are gamma dose-rates from <2 mm and >2 mm size fractions, respectively, and x represents the mass fraction of <2 mm size fraction. Moisture attenuation (beta and gamma) and grain size and etching (beta) factors were applied to derive final beta and gamma dose-rates (Zimmerman, 1971). The total dose-rate included an estimated internal alpha dose rate of 0.010 ± 0.002 mGya^{-1} (Vandenberghe et al., 2008).

3.3. Determination of vertical displacements and uplift rate

The uplifted marine terraces observed in the northeastern Pontides between Trabzon and Rize is assumed to record the Quaternary-Holocene sea-level changes which happened during the odd numbered MIS stages. To estimate the uplift rate, the chronology of the marine terraces in is based on the correlation with the nearest sea-level highstand (e.g., Saillard et al., 2009; Roberts et al., 2013; Jara-Muñoz et al., 2015; Pedoja et al., 2018). Because of this, we calculated the vertical movement of the marine terraces (E-e), using the difference between the present-day elevation and the old elevation or eustatic sea-level estimates, and applying the following equation (Lajoie, 1986) to each marine terrace to estimate an uplift rate. The uplift rate can also be determined without the old elevation as an apparent rate (Pedoja et al., 2011; Pedoja et al., 2018; Normand et al., 2019).

$$(U)\ \text{Uplift Rate} = (E-e)/A,$$

where "E" is the present-day elevation of the marine terrace level, "e" is the old elevation of the marine terrace level, and "A" is the age of the marine terrace from the correlation with the marine isotope stages. To calculate precise uplift rates and error propagations, we used a modified version of the uplift rate formula incorporating the different eustatic sea-level uncertainties like marine terrace studies which were used by Pedoja et al. (2018) and Normand et al. (2019).

$$U_{min} = [(E-\Delta E)-(e+\Delta e)]/(A+\Delta A),\ U_{max} = [(E+\Delta E)-(e-\Delta e)]/(A-\Delta A)$$

$$\Delta U = |U|\sqrt{(\Delta A/|A|)^2+((\sqrt{\Delta E^2+\Delta e^2})/(|E-e|)^2},$$

where the delta symbols represent the estimated variability in the different parameters. We also used the marine record (Siddall et al., 2006 and Spratt and Lisiecki, 2016) to correlate these highstands with our chronology.

4. Results

4.1. Field work in marine terraces

We identified three terraces in the field: T1, T2, and T3. These terrace levels have a high discrepancy in the elevation of their top surfaces such as T3 (3–27 m), T2 (35–45 m), and T1 (48–60 m) above the sea-level. The terrace deposits consist mainly of clays, silts, sands and gravels and have thicknesses ranging from 1 to 17 m. The deposits are made up of mostly gravels derived from basaltic, andesitic, and limestone and these gravels are of ellipsoidal, square and flat shapes. The terraces are overlain by brownish-gray soil. Even though all terrace deposits generally appear very similar, majority of the features (micro fossil faunas, cement type, colors, altitudes, etc.) vary significantly. Because of this, we identified three marine terrace levels based on the sedimentology and morphostratigraphy of these deposits as mentioned above. These marine terraces increase in height and thickness from west to east, and they are displaced by normal faults. Micropaleontological observations indicate that T2 terrace has marine benthic foraminifera. It has a planispiral-evolute coiling shape. Because of the paucity of the fauna, the specific kind of foraminifera could not deeply be characterized. In addition to that, Keskin et al. (2011) defined marine macro gastropods in their lowest four terrace deposits in the Trabzon.

The T3 terrace is only exposed in the center of the Yomra (Trabzon) district. T3 terrace is located at between 3 m and 27 m elevation above sea-level. This section is characterized by sedimentary deposits, ranging from 1 to 4.5 m thick, poorly to moderately sorted gravels and containing an upward-fining sand succession (Figures 4a and 4b). The bottom of this section consists of coarse sand and mud with a thickness of 2 m. Overlying these are beds consisting of intercalated medium to coarse sand and clay with a thickness of 1 to 2 m. The present shoreline angle of the T3 terrace has a maximum altitude of 27 m (varies

between 3 m and 27 m), and it can be traced laterally for around 200 m. One OSL sample was collected from the top unit of this site: TR-9, at a depth of 265 cm.

Outcrops of T2 terrace is observed in the Yalıköy (Trabzon), Keremköy (Trabzon), Söğütlü (Trabzon), Yalıncak (Trabzon, three sites), Yalıköy (Rize) districts and in Rize city. T2 terrace is located at between 35 m and 45 m elevation above sea-level. The present shoreline angle of T2 terrace has an average altitude of 40 m, and it can be traced laterally in the 8 districts for distances ranging from 100 to 200 m. The T2 terrace consists of a moderate to poorly sorted 1 m thick clast-supported gravel beds (Figures 4c and 4d). This section comprises fining upwards sedimentary deposits with a thickness of up to 7 m and fines upward. The bottom of the section comprises coarse gravel, sand and mud with a thickness of 1 m. Above this the section consists of medium to coarse sand and clay beds, ranging from 1 to 2 m thick. Microfossils were discovered in the sandy levels of the T2 terrace (Figure 4d, inset). Eight OSL samples were collected from outcrops of T2 terrace: TR-2, TR-4, TR-5, TR-6, TR-7, TR-8, TR-12, and TR-13 at depths of 240, 130, 230, 210, 440, 280, 260, and 220 cm, respectively.

The T1 terrace is observed in the Yıldızlı (Trabzon, two sites) district. T1 terraces is located at between 48 m and 60 m elevation above sea-level. This section is composed of deposits with a thickness of approximately 8 m. The bottom of this section consists of a 1 to 3 m thick coarse conglomerate and sand, followed by a 1 to 4 m thick fine to coarse sand (Figures 4e and 4f). The 0.5 to 2 m thick sand layers have no structure patterns. The T1 marine terrace can be traced laterally at the two sites for 100 to 200 m. One OSL sample per site was collected from each site: TR-1 from the Yıldızlı site (hanging wall of the fault) and TR-3 from the Yıldızlı site (footwall wall of the fault) at depths of 225, and 120 cm, respectively.

4.2. Chronology of marine terraces

OSL dating results are shown in Table 2. Nine of the samples had sufficient specific sensitivity to enable measurement of 1 mm aliquots; for the remaining 2 samples (TR-2 and TR-13) 3 mm aliquots were measured. Dose recovery tests indicated optimized preheat treatments ranging from 220 °C to 280 °C for 10 s; a 160 °C cutheat was used for all measurements. Six of the samples (TR-1, TR-3, TR-6, TR-7, TR-8, and TR-13) passed SAR acceptance thresholds at the 75% or greater level, whereas the remaining 5 samples only had 25%–50% aliquot acceptance. This latter group was dominated by poor recycling or recuperation data, and for 3 of the samples (TR-4, TR-5, and TR-9) resulted in low numbers of accepted aliquots. All the SAR D_e data for sample TR-9 failed the 5% acceptance threshold for recuperation tests. The SAR data were reanalyzed using the early background subtraction (signal 0–0.8 s, background 0.8–2.72s) method (Cunningham et al., 2015), but recuperation data remained above the 5% threshold. SAR data for TR-9 using the original late background subtraction analysis was reanalyzed with a 15% recuperation acceptance threshold.

In dose distribution assessment we used a similar approach to Johnson et al. (2019) by comparing overdispersion (σ_b) data calculated from our samples (Table 2; Figure 5) to factorial experiments using what were considered to be well-bleached samples (Galbraith et al., 2005). We estimate our 125–180 μm quartz discs comprised ~30 or ~260 grains for 1 mm or 3 mm diameter aliquots, respectively. As described in detail by Galbraith and Roberts (2012), determination of De using central age model (CAM) can be reliable only if the dispersion (OD) value of measurements lies within an acceptable range (20%–30% maximum). In this assessment, overdispersion values for all our samples exceed values from Galbraith et al. (2005) (with estimated modifications of their data for numbers of grains and aliquot size), and all of the samples analyzed here would be expected to exhibit some level of partial bleaching. This was somewhat expected given the 1–2 cm clasts observed in a number of the samples, with an interpretation of the higher level of energy and rapidity of sedimentary deposition, resulting in poor to moderate sorted. Accordingly, as a first step we analyzed the data using MAM. For 3 of the samples (TR-1, TR-2, and TR-6) the MAM analysis was repeated after removing lowest D_e values, and in each case the P-value appreciably increased. The MAM results were further reanalyzed by inflating the instrumental uncertainty from 1.5% to 3% (Spencer et al., 2015); this only made an appreciable difference in the analysis for sample TR-6. For 2 of the samples (TR-8 and TR-13) the MAM analysis had very low P-values, and for these 2 samples the CAM result is reported. The result from the initial MAM analysis was then examined visually on radial plot diagrams, together with an assessment of the asymmetric or symmetric nature of the D_e data (Figure 5), and a comparative evaluation to other sample ages and terrace location. Based on these dose distribution analysis steps either a MAM or CAM D_e result was chosen (Table 2, Figure 5).

For samples TR-12 and TR-13 a Cs-137 peak was positively identified by gamma spectrometry. Its specific activity is low, 1.0 ± 0.2 and 4.3 ± 0.3 $Bqkg^{-1}$, respectively. These are significantly higher than the minimum detectable activity, defined by the upper limit observed from other samples in this project (Gilmore, 2008). The source of the Cs-137 is somewhat difficult to determine, as this is an anthropogenic nuclide produced from nuclear weapon testing and nuclear power plant accidents. The laboratories that handled these samples process the occasional modern sample, but none were being processed at the time we analyzed the TR samples discussed here. Although it is hard to completely discount a laboratory contamination,

Figure 4. a) View of the OSL sampling location in the T3 Terrace level near Yomra city. b) View of the actual sediment. The red dashed line indicates wave-cut notch of the paleoshoreline. c) View of the OSL sampling location in the T2 terrace level near Keremköy village. d) View of the 3 to 4 m T2 marine terrace and sampling location. Inset view depicts a marine foraminifer in the T2 terrace level. e) and f) View of the OSL sampling location in the T1 marine terrace. g) View of the marine terraces on the coast of the Eastern Pontides.

Table 2. Quartz OSL data and ages for marine terraces between Trabzon and Rize, Turkey.

Sample ID	Terrace level	Overburden depth (m)	Water content[a] (%)	Aliquot size[b] (mm)	Preheat[c] (°C)	n[d]	OD[e] (%)	Equivalent dose, D_e[f](Gy)	Dose-rate (Gy/ka)	OSL age (ka)
TR-3	T1	1.20	4.0 ± 5.0	1	220	18 (24)	31.9	57.7 ± 4.5[c]	1.10 ± 0.04	52.4 ± 4.6
TR-1		2.25	9.5 ± 5.0	1	280	21 (24)	26.8	54.0 ± 3.6[m]	0.90 ± 0.04	60.0 ± 4.7
TR-7	T2	4.40	17.1 ± 5.0	1	220	31 (40)	47.0	66.8 ± 5.7[c]	2.06 ± 0.19	32.4 ± 4.0
TR-8		2.80	16.5 ± 5.0	1	220	35 (44)	44.4	91.4 ± 6.9[c]	2.78 ± 0.10	33.9 ± 2.8
TR-5		2.30	8.3 ± 5.0	1	260	12 (24)	52.4	54.3 ± 5.1[m]	2.34 ± 0.10	22.5 ± 2.3
TR-6		2.10	5.9 ± 5.0	1	220	19 (24)	34.1	44.4 ± 1.5[m]	1.60 ± 0.07	27.7 ± 1.5
TR-2		2.40	10.3 ± 5.0	3	240	17 (48)	46.0	53.2 ± 6.1[c]	2.21 ± 0.09	24.0 ± 2.9
TR-4		1.30	12.9 ± 5.0	1	280	10 (44)	65.3	39.6 ± 3.5[m]	1.52 ± 0.06	26.1 ± 2.5
TR-12		2.60	11.2 ± 5.0	1	260	17 (68)	35.3	41.3 ± 3.8[c]	1.99 ± 0.09	20.7 ± 2.0
TR-13		2.20	9.8 ± 5.0	3	220	41 (41)	15.5	46.8 ± 1.2[c]	2.78 ± 0.11	16.8 ± 0.8
TR-9	T3	2.65	10.4 ± 5.0	1	260	11 (40)	29.6	24.5 ± 1.7[m]	2.09 ± 0.08	11.7 ± 0.9

[a]For most samples estimates of field moisture determined when samples were collected was used, and in these instances the field and estimated saturation level were similar or consistent within the given uncertainty level. For samples TR-1 and TR-7 there was greater disparity between field and saturated values, and to account for this the estimated water content over the burial period for these samples was adjusted.

[b]All quartz grains analyzed were 125–180 μm in size. Estimated numbers of grains are ~30 or ~260 on 1 mm or 3 mm aliquots, respectively.

[c]Preheat chosen from dose recovery tests and used for D_e replication; cutheat was 160 °C for all measurements.

[d]Number of aliquots of D_e measurement that passed threshold limits (recycling, recuperation) and used to estimate final D_e. Figures in parenthesis indicate total number of aliquots measured. For sample TR-9, recuperation threshold for accepted aliquots was set at 15%.

[e]Over-dispersion in D_e data.

[f]Superscript 'c' indicates CAM result; superscript 'm' indicates MAM result. See text for details of results and discussion.

Cs-137 has never been observed in the gamma spectra of non-modern samples analyzed by these laboratories before. Also, given the sequential analytical procedures employed we would expect to observe evidence of these peaks in most if not all of the samples analyzed here. In addition, we also observed a Cs-137 peak for the larger than 2 mm grain size fraction of sample TR-13; the sample that has the highest activity for Cs-137. The larger than 2 mm fraction has a 1.1 ± 0.2 $Bqkg^{-1}$ activity. It is lower, for a larger grain size, which makes sense if this Cs-137 contamination came from the environment. On balance, the source of the Cs-137 is more likely to be at the sampling sites themselves, possibly transported from surficial (modern) deposits to the sediment samples for OSL either by infiltrating waters or bioturbated clays, silts, or fine sands. The sediment prepared for gamma spectrometry measurement was taken from the OSL cylinder ends; an alternative would be that the Cs-137 is only present at the surface, such as the outcrop, thus present at the end of the OSL cylinder. Fortunately, the presence of Cs-137 has a negligible effect on the dose-rate for the samples discussed here, if only for the very short duration of exposure, compared to their total burial age. However, if this contaminant carried with it very fine sands it would point to a possible source of modern contamination that could result in a lower D_e value and thus underestimate the true depositional age. Samples TR-12 and TR-13 do have the two lowest OSL ages (20.7 ± 2.1 ka and 16.8 ± 0.8 ka, respectively; Table 2) for the group of samples from terrace level T2, but they are not significant outliers given the range in age (22.5 to 27.7 ka; Table 2) for the other T2 samples and should not be excluded for this reason.

The OSL ages for the marine terraces (Table 2), broadly cluster into 3 groups with ages of 11.7 ka (terrace level T3), 16.8 to 33.9 ka (T2), and 52.4 to 60.0 ka (T1), and at altitudes ranging from 3–27 m (T3), 35–45 m (T2), and 48–60 m (T1), respectively, (Table 3, Figure 6).

4.3. Vertical displacement and uplift rates of marine terraces

Based on the established OSL chronology, the terraces were assigned to MIS 3c, MIS 3a and MIS 1. The apparent vertical movement rates range from 1.50 mm/year to 0.98 mm/year. The uplift rate results are 0.98 ± 0.12 mm/year, 1.39 ± 0.26 mm/year, and 1.50 ± 0.78 mm/year, as calculated from marine terrace level 1, 2, and 3, respectively (Table 4). After incorporating the eustatic sea-level estimations based on the Spratt and Lisiecki (2016), the uplift rates were estimated as 2.13 mm/year, 4.88 mm/

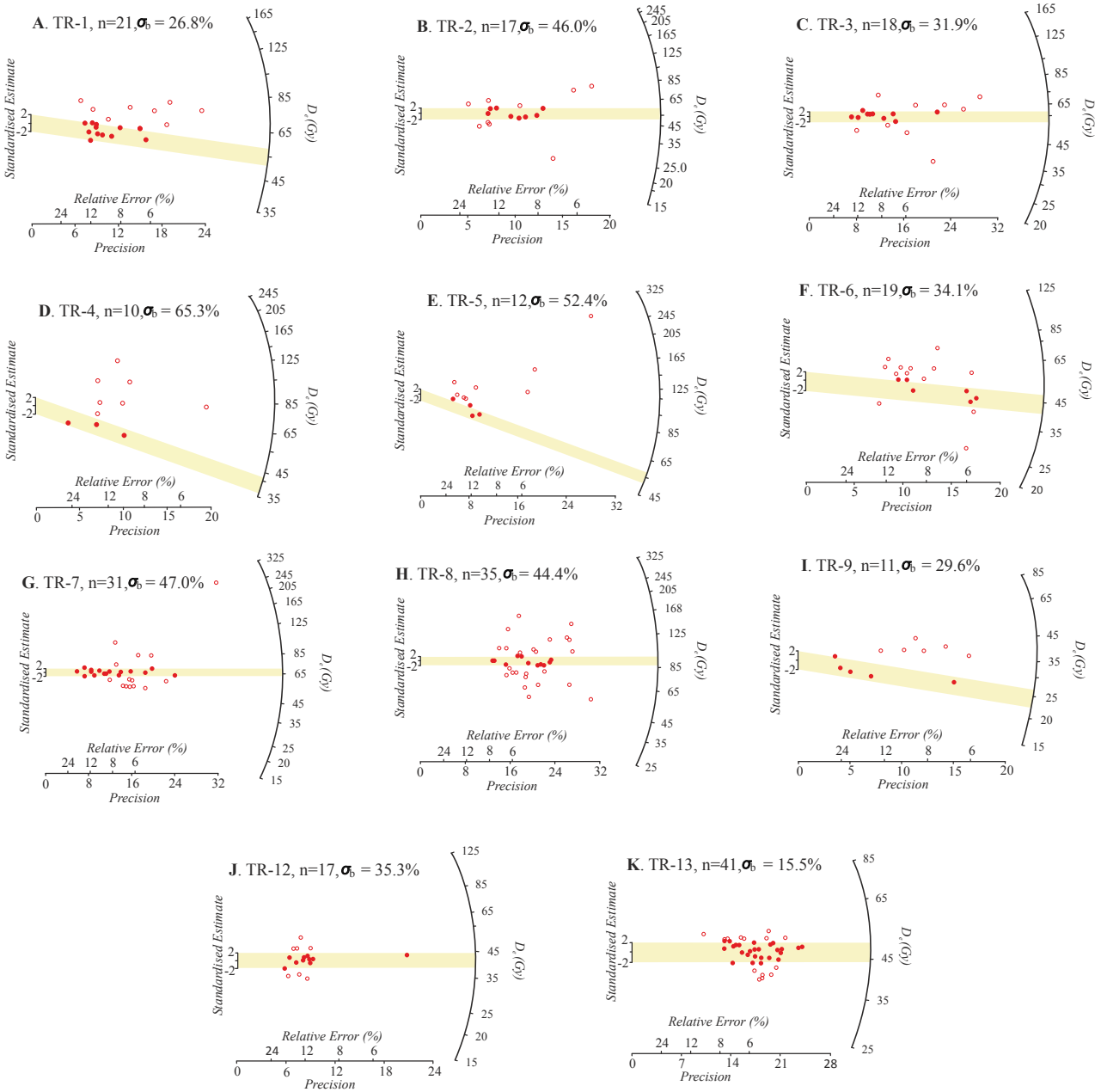

Figure 5. Radial plots of D_e data. Open circles are individual D_e estimates, with each value read by projecting a radial line from the y-axis origin (on the left) through the point to the radial axis on the right, and corresponding standard error read by extending a line vertically to the x-axis; n is number of accepted quartz aliquots with individual D_e values; σ_b is percent overdispersion. The light yellow band indicates the age model result, the ±2-unit width of which indicates a 2σ confidence interval. All radial plots are aligned in the horizontal with the CAM result; if the light yellow band dips below the horizontal the MAM result is indicated.

year and 3.96 mm/year, respectively, (Table 4). The uplift rate estimations show a gradual increase during a short time interval. In the Eastern Pontides, multiple normal faults displaced the deposits (Figure 6). Albeit these faults contribute to regional subsidence of the coastal region of Eastern Pontides, our results indicate a differential uplift along the coast.

5. Discussion

5.1. Chronology of marine terraces

Many marine terraces have been studied in the northeast region of the Black Sea and the Caspian Sea, where the active deformation is in progress. Especially Russia, Ukraine, and Baku region holds well-preserved marine

Table 3. Spatio-temporal positions of the terraces.

Terrace	OSL ages- A (ka)			Shoreline angle elevation E ± ΔE (m)			Sediment thickness (m)
	A_{min}	A_{max}	$A_{average}$	E_{min}	E_{max}	$E_{average}$	
T1	52.4 ± 4.6	60 ± 4.7	56.2 ± 4.65	48 ± 5	60 ± 4	54 ± 4.5	2.25
T2	16.8 ± 0.8	33.9 ± 2.8	25.5 ± 2.35	35 ± 3	43 ± 2	39.4 ± 2.9	4.4
T3	11.7 ± 0.9	11.7 ± 0.9	11.7 ± 0.9	3 ± 1*	27 ± 3	15 ± 2	2.65

* Actual terrace at the present shoreline angle, as observed in the field (see Figure 4b and text).

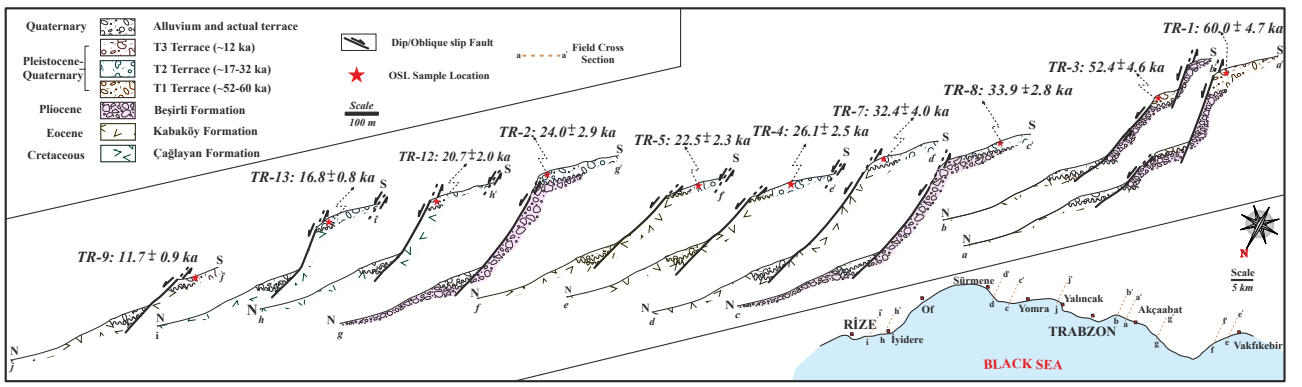

Figure 6. The crosssections of uplifted marine terraces between Trabzon and Rize are compared along the Southeast Blacksea Fault (modified from Softa et al, 2019).

Table 4. Marine isotope stages and uplift rate calculation of marine terraces.

Terrace	Assigned MIS stage	Assigned MIS age[a] A ± ΔA (ka)	Shoreline angle elevation E ± ΔE (m)	Apparent uplift rate U = E/A (mm/year)			Eustatic estimations[b] (m)			Uplift ranges U = E-e/A (mm/year)				
				U_{max}	U_{min}	U ± ΔU	e	+Δe	−Δe	Umax	Umin	U	+ΔU	−ΔU
T1	3c	55 ± 6	54 ± 4	1.18	0.82	0.98 ± 0.12	-63	8	19	2.86	1.72	2.13	4.77	2.77
T2	3a	28 ± 5	39 ± 3	1.83	1.09	1.39 ± 0.26	-97.5	10.5	14.5	6.70	3.73	4.88	7.16	5.27
T3	1	10 ± 5	15 ± 2	3.40	0.87	1.50 ± 0.78	-24.6	14.7	25.8	13.44	1.53	3.96	5.03	4.74

[a]MIS letters and ages and defined by Siddal et al. (2006); Railsback et al. (2015). [b] Eustatic estimations based on the Spratt and Lisiecki (2016) and positive and negative error (Δ) based on the bootstrapping results, 97.5% and 2.5% respectively.

terraces that incorporates macro and micro fossil faunas (e.g., Nesmeyanov, 1995; Zubakov, 1998; Panin and Popescu, 2007; Yanina, 2012, 2013; Kurbanov et al., 2014; Zastrozhnov et al., 2020). However, these terraces were dated to Pleistocene to Holocene time interval, which indicate a discrepancy with respect to fossil faunas when compared to the eastern Black Sea terraces. As our chronology between 11.7 to 60 ka, these terraces attributed to MIS 1, MIS3a, and MIS3c (Figure 7). Similarly, Choi et al. (2003a, 2003b) report broad clusters of ages with varying terrace altitude (50–70 ka and ca. 110 ka with 7–25 m.a.s.l. for their terrace #2) in their SAR OSL dating of marine terraces in Korea. Choi et al. (2003a, 2003b) interpret the varying terrace altitude across their study area supportive of considerable tectonic activity in the Late Pleistocene. Moreover, Kurbanov et al. (2014) dated the marine terrace succession with a radiocarbon age of 12–14 ka in the east of the Caspian Sea. The terraces levels of the Russian coast dated with the radiocarbon method with the age of 30–40 ka (Zubakov, 1988). Also, Zubakov and Kochegura (1974) and Sudakova et al. (1977) dated with the thermoluminescence dating the marine terraces in the north of the Black Sea (Russia). Their age results ranging from 15 to 37 ka.

In addition to the Black sea region, marine terraces in Hatay along the Mediterranean coasts were dated using

ESR dating with ranged from 0.2 to 256 ka (Florentin et al., 2014). Similarly, in the same region, marine terraces were dated using the ESR dating between 8.3 and 214 ka (Tarı et al., 2018). Tarı et al. (2018) reported most of the dated terraces contained mollusks reworked from several earlier deposits due to later tectonic movements, sea-level fluctuations, and associated sedimentary processes. Also, Nalin et al. (2020) dated using the infrared-stimulated luminescence (IRSL) dating the marine terraces on the Mediterranean coast (southern Italy). Their IRSL ages range from 64 ka to >240 ka with varying terrace altitude (3.5–225 m.a.s.l).

Similarly, the SAR OSL ages presented here indicate such differential uplift for the coastal northeastern Pontides region where terraces have been displaced by normal faults (e.g., Softa et al., 2019) (see Figure 6). However, Keskin et al. (2011) reported ages of up to 416.2 ± 92.7 ka, 292.5 ± 49.8 ka and 124.8 ± 26.0 ka for our T1, T2 and T3 levels, respectively using ESR dating of gastropods. Albeit we collected 11 samples including Keskin et al.'s (2011) sites, although we encountered few marine foraminifers during the micropaleontological analysis, we did not find any fossils suitable for amino acid racemization analysis and ESR dating. Ideally, macrofossil faunas such as shells are more common in marine terraces at the open systems and thus may be subject to postdepositional contamination that prevents their use as dating material (e.g., Ortlieb et al., 1992; Pedoja et al., 2006). Given the numerous intrinsic tests of the luminescence characteristics and detailed environmental radioactivity assessment, we would argue that the OSL indicates sedimentary depositional ages of ≤ 60 ka (Figure 7).

The Black sea shows marine conditions during MIS 1 and MIS 3 (e.g., Aksu et al., 2002), is contrary to the findings of Yanko-Hombach et al. (2007); Panin and Popescu (2007); Ryan et al. (2003); Yanchilina et al. (2017); Yanina (2014) and Krijgsman et al. (2019). The majority of these studies argued for lacustrine conditions during MIS 3 based on the radiocarbon dating of sediment cores. However, MIS 3 high stand is still under debate, the sea-level drop is estimated ranging from 10 to 40 m, as evidenced by marine terraces in the Caucasian and Romanian coast at the Black sea (Panin, 1983; Chepalyga, 1984; Panin and Popescu, 2007). In addition, some studies investigated the paleo-salinity rate of the Marmara Sea and the Black Sea to evaluate the connection times (e.g., Aksu et al., 2002; Soulet et al., 2010; Nowaczyk et al., 2012; Çağatay et al., 2015; Aloisi et al., 2015). Although $CaCO_3$, Cl^- and

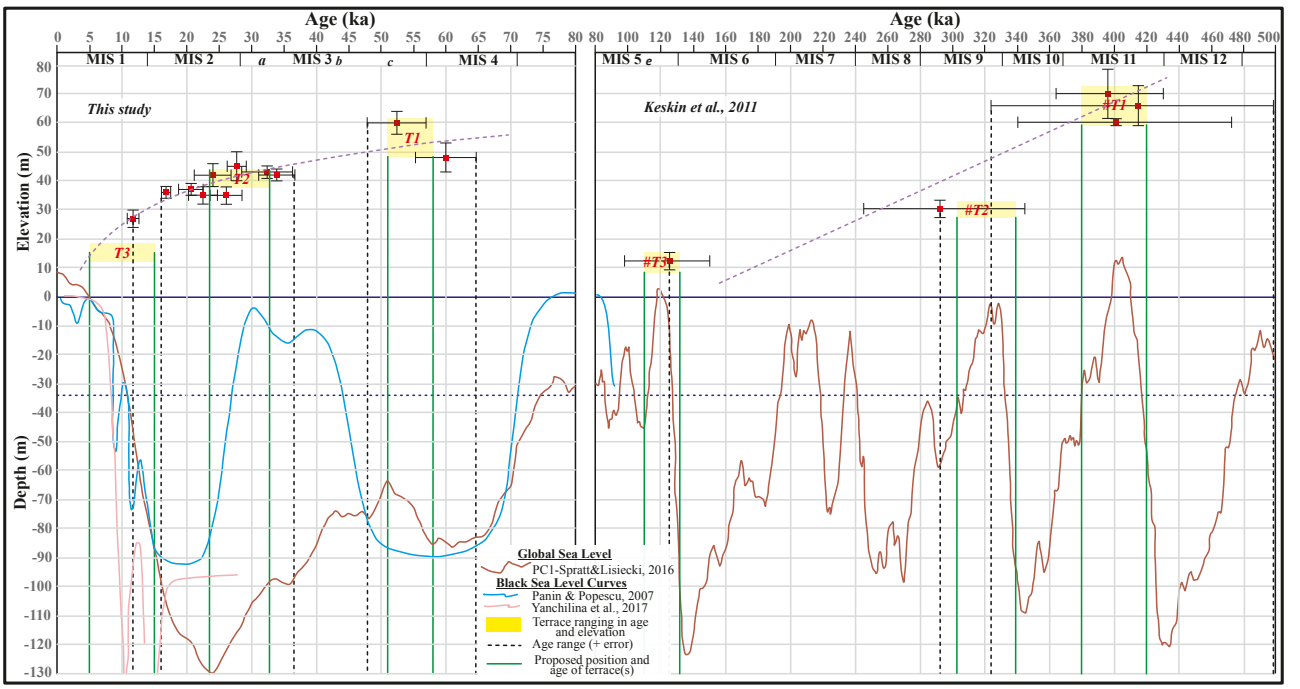

Figure 7. Correlation of marine terrace cycles with the Global and Black Sea level changes along with the Eastern Pontides (Plot adopted from Erturaç, 2020, and the published chronology is compiled from Keskin et al., 2011). The yellow boxes reflecting variations in age and vertical positions (m.a.s.l), ages and positions of OSL samples and global relative sea-level curve (PC1, Spratt and Lisiecki, 2016) and Black Sea level curve (Panin and Popescu, 2006 and Yanchilina et al., 2017). Dashed black lines indicate extend of the ages attributed to a certain terrace level and green lines are used to correlate the proposed terraces to sea-level curves. Dashed horizontal line indicates ~-35 m sill depth of the Bosphorus.

Ca measurements cannot be used directly determining paleo-salinity, these specific data can reflect characteristics of the water bodies (Yanchilina et al., 2017). Aloisi et al. (2015) stated that the Marmara Sea was not freshwater [Salinity = 4 psu (practical salinity unit)] during MIS 3. Moreover, as evidence of marine conditions during MIS 3, we have found a marine foraminifer in T2. Thus, it can be deduced that marine conditions prevailed in the Black Sea during MIS 3. But this finding is still needed to be verified by detailed paleontological studies that should define the characteristic of fossil faunas in the southeastern Black Sea coasts.

Keskin et al. (2011) recorded the MIS 5e, which was significant sea-level changes in the eastern Black Sea region. But we did not encounter MIS5e in the marine terraces. Considering our robust OSL chronology, this is possibly related to Keskin et al.'s (2011) ESR chronology. However, some studies observed MIS 5e in the closer region eastern Black sea such as Central Pontides and north of the Black Sea (Nesmeyenav, 1995; Zubakov, 1998; Panin and Popescu, 2007; Yildirim et al., 2013). This can be explained by four reasons; (i) tectonic factors may temporally were dominant, (ii) the anthropogenic erosion of marine terraces due to urbanization and agricultural activities, (iii) discrepancy in chronology dependent on the applied dating technique, and (iv) morphological evolution of the marine terraces in the coastal region of Eastern Pontides. We interpret that marine terrace evolution is mainly related to the tectonic process and rapid uplift.

5.2. Evaluation of uplift rates, vertical movement and seismic activity

To constrain uplift rate, we used the elevations of the dated of marine terraces. According to our results the formation marine terraces was strongly associated with Quaternary regional uplift and sea-level changes. Uplift rates of the coastal Western, Central, and Eastern Pontides have previously been calculated by Erturaç (2020), Yildirim et al. (2013), Berndt et al. (2018), Erturaç and Kıyak (2017), Keskin (2007), and Keskin et al. (2011) from OSL and ESR ages of fluvial and marine terraces. From studies of raised fluvial and marine terraces in the Sakarya region, Sinop Peninsula, Samsun region, and Amasya region, more than 400km west of our study area, uplift rates 0.78 ± 0.03 mm/year (Erturaç, 2020), between 0.04 ± 0.01 mm/year and 0.23 ± 0.04 mm/year (Yildirim et al., 2013), 0.28 ± 0.07 mm/year (Berndt et al., 2018), and 0.94 ± 0.26 mm/year (Erturaç and Kıyak, 2017) were calculated. Except for these local uplift rate studies, Okay et al. (2020) stated that central Anatolia was uplifted less than 0.05 km/Myr since 41 Ma in the light of the previously published papers, as well as new thermochronological data. From previous work in the Trabzon area, the mean uplift rates were calculated as 0.62 ± 0.01 mm/year to 1.34 ± 0.06 mm/year (Keskin, 2007) and 0.07 ± 0.05 mm/year to 0.17 ± 0.03 mm/year Keskin et al. (2011). Considering the high relief in the Eastern Pontides, these uplift rates are slightly lower than our own results. This eastward regional increase in uplift rates as a factor of two along the Black Sea coast may be explained not only by the distance from the NAF's and NEAF's main strand and strain accumulation along the coast (Berndt et al., 2018) but it also of the material used (mineral, fossils, etc.) for dating methods depend on whether related to postdepositional contamination and fluvial reworking or not. This differentiate uplift can be interpreted to be related to the asymmetrical uplifting along the NEAF, the KF, and BKF. Ideally, the higher uplift rates should be expected in the northeastern Pontides.

The cause of the higher uplift rates in the Eastern Pontides might be associated with global tectonic processes linked with a push up structure within the BSF in the sea and the BKF on land in conjunction with the NAF (e.g., Softa et al., 2018, 2019). In addition, the Kazbegi-Borjomi thrust fault is the part of NEAF, (e.g., Philip et al, 1989). Moreover, Altıntaş (2014) stated that the Eastern Pontides has been drifting northeasterly direction based on GNSS measurement, which is the biggest deformation values up to 6.2 mm on the north axis, and up to 17.4 mm on the east axis between Trabzon and Gümüşhane. This GNSS data is consistent with our proposed uplift model.

According to our field studies, the marine terraces have displaced at least 50 m by the Southeast Black Sea Fault. In the light of geomorphic data, field evidence and our OSL chronology, we suggest that the Southeast Black Sea Fault is active. However, the earthquakes were generated by this fault is still under discussion. This displacements can be caused by more than one large earthquake and/or continuously aseismic creeping along the fault surfaces. As the Southeast Black Sea Fault is a normal fault, we expect that earthquakes related to normal fault mechanism. But we did not identify any earthquake related to normal fault among the documented over the fifty earthquakes with magnitude higher than 4 between 1900 and 2020[1]. Given the tectonic structure of the Eastern Pontides, a plausible scenario is that the unidentified earthquakes related to Southeast Black Sea Fault is probably responsible for the aseismic creeping (Softa et al., 2019; Nas et al., 2020). Although aseismic creep is more frequently observed on strike-slip faults (Schulz et al., 1982; Sieh and Williams, 1990; Karabacak et al., 2011) such as San Andreas Fault Zone and North Anatolian Fault Zone, this phenomenon is also reported for normal faults (Hreinsdóttir and Bennett, 2009; Özkaymak et al., 2019). In addition, Maden and Öztürk (2015) stated that the lowest b values were

[1]ISC (International Seismological center) (2020). Recent Earthquakes in Turkey [online]. Website http:// http://www.isc.ac.uk/ [accessed 20 October 2020].

obtained among the NAF, the eastern Anatolia, and Black Sea. These data confirm the higher strain and higher uplift rate within the area. In brief, Keskin et al.'s (2011) study and our study are pioneers in reconstructing the chronology of the marine terraces in the Eastern Pontides and more studies needed to refine the existing knowledge.

6. Conclusion

We have examined sediments from a sequence of emerged marine terraces that are located on the coastal region of the Eastern Pontides, on the push-up system, between the Black Sea Fault and the Borjomi-Kazbegi Fault. The OSL samples were collected from 3 marine terraces which have heights ranging from 3 to 60 m. These deposits have displaced by an active normal faults. Luminescence behavior was mixed with 5 of the 11 samples failing recycling and recuperation test thresholds, resulting in limited numbers of accepted D_e values for these samples. Three different terrace sedimentation periods have been determined, one at 11.7 ka, one between 16.8 to 32.8 ka and the last one at 52.4 to 60 ka.

Based on the stratigraphy and the geomorphology of the study area, marine terraces of currently equal altitude are of the same age. Our result is consistent with the usual evolutionary model of a terraced sequence, moving from the highest to the lowest elevation. Based on the obtained OSL ages, we correlate each terrace level with the marine isotope stage/substage. The terraces are assigned to MIS 3c, MIS 3a and MIS 1. While the measured Late Quaternary apparent uplift rate ranges from 0.9 mm/year to 1.5 mm/year, after the eustatic sea-level estimations, the surface uplift rate ranges from 2.13 mm/year to 4.88 mm/year and is probably related to tectonic processes. These tectonic processes might be associated with tectonic push up deformation between the Black Sea Fault and the Kazbegi-Borjomi thrust faults. Moreover, movements of these faults have accommodated higher uplift rates over the Late Quaternary.

Acknowledgments

This work is part of a Ph.D. thesis undertaken by Mustafa Softa at the Institute of Natural and Applied Sciences, Dokuz Eylül University, Turkey. This study is funded by Dokuz Eylül University Research Projects "DEU-BAP-2014.KB.FEN.044". The first author was supported by the International Research Fellowship of the Scientific and Technological Research Council of Turkey (TÜBİTAK). The manuscript was edited by Elsevier Language Editing. The authors would like to thank the anonymous reviewers for their critical and constructive comments that greatly contributed to improving the final version of the paper. Special thanks are due Dr. Emine Türk Öz for palaeontologic evaluations. The authors express their appreciation to the guest editor for useful comments that greatly helped to improve an earlier version of the manuscript and the main editor for considering our paper for publication.

References

Adamia SA, Lordkipanidze MB, Zakariadze GS (1977). Evolution of an active continental margin as exemplified by the Alpine history of the Caucasus. Tectonophysics 40: 183-189.

Aitken MJ (1985). Thermoluminescence Dating. London, UK: Academic Press.

Aitken MJ (1998). An Introduction to Optical Dating. London, UK: Oxford University Press.

Aksu AE, Hiscott RN, Kaminski MA, Mudie PJ, Gillespie H et al. (2002). Last glacial-Holocene paleoceanography of the Black Sea and Marmara Sea: stable isotopic, foraminiferal and coccolith evidence. Marine Geology 190: 119-149.

Altıntaş F (2014). Determining the current tectonic movements during the Line Gümüşhane-Trabzon with GNSS data. Master Thesis, Gümüşhane University, Gümüşhane, Turkey (in Turkish).

Ardel A (1943). Trabzon ve civarının morfolojisi üzerine gözlemler. Türk Coğrafya Dergisi 1: 71-82 (in Turkish).

Avagyan A, Sosson M, Karakhanian A, Philip H, Rebai S et al. (2010). Recent tectonic stress evolution in the Lesser Caucasus and adjacent regions. Geological Society of London Special Publications 340: 393-408.

Aytac A (2012). An approach to the sea level changes to base on the marine terraces of the Turkish Black Sea coasts. Quaternary International 30: 279-280.

Badertscher S, Fleitmann D, Cheng H, Edwards RL, Göktürk OM et al. (2011). Pleistocene water intrusions from the Mediterranean and Caspian seas into the Black Sea. Nature Geoscience 4: 236-239. doi: 10.1038/ngeo1106

Badgley PC (1965). Structural and Tectonic Principles. New York, NY, USA: Harper International Press.

Bateman MD (2015). The application of luminescence dating to sea-level studies. In: Shennan I, Long AJ, Horton BP (editors). Handbook of Sea-level Research. Chichester, USA: American Geophysical Union, pp. 404-420.

Bektaş O, Yılmaz C, Taslı K, Akdag K, Ozgur S (1995). Cretaceous, rifting of the eastern Pontide carbonate platform (NE Turkey): the formation of carbonate breccias and turbidites as evidence of a drowned platform. Giornale di Geologia 57 (1-2): 233-244.

Bektaş O, Şen C, Atıcı Y, Köprübası N (1999). Migration of the Upper Cretaceous subduction related volcanism towards the back-arc basin of the eastern Pontide magmatic arc (NE Turkey). Geological Journal 34: 95-106.

Berndt C, Yıldırım C, Çiner A, Strecker MR, Ertunç G et al. (2018). Quaternary uplift of the northern margin of the Central Anatolian Plateau: New OSL dates of fluvial and delta-terrace deposits of the Kızılırmak River, Black Sea coast, Turkey. Quaternary Science Reviews 201: 446-469.

Beukens RP (1994). Procedures and precision in ^{14}C AMS. Nuclear Instruments and Methods in Physics Research Section B: Beam Interactions with Materials and Atoms 92 (1-4): 182-187.

Bøtter-Jensen L, Andersen CE, Duller GAT, Murray AS (2003). Developments in radiation, stimulation and observation facilities in luminescence measurements. Radiation Measurements 37 (4-5): 535-541.

Chepalyga AL (1984). Inland Sea Basin. Late Quaternary Environments of the Soviet Union. In: Velichko AA, Wright Jr. HE, Barnowsky CW (editors). English ed. Minneapolis, MN, USA: University of Minnesota Press, pp. 229-247.

Choi JH, Murray AS, Cheong CS, Hong DG, Chang HW (2003a). The resolution of stratigraphic inconsistency in the luminescence ages of marine terrace sediments from Korea. Quaternary Science Reviews 22: 1201-1206.

Choi JH, Murray AS, Jain M, Cheong CS, Chang HW (2003b). Luminescence dating of well-sorted marine terrace sediments on the southeastern coast of Korea. Quaternary Science Reviews 22: 407-421.

Cunningham AC, Wallinga J, Hobo N, Versendaal AJ, Makaske B et al. (2015). Re-evaluating luminescence burial doses and bleaching of fluvial deposits using Bayesian computational statistics. Earth Surface Dynamics 3: 55-65.

Çağatay MN, Wulf S, Sancar Ü, Özmaral A, Vidal L et al. (2015). The tephra record from the Sea of Marmara for the last ca. 70 ka and its palaeoceanographic implications. Marine Geology 36: 96-110.

Dewey JF, Pitman WC, Ryan WBF, Bonnin J (1973). Plate tectonics and evolution of the Alpine system. Geological Society of America Bulletin 84: 3137-3180.

Duller GAT (2003). Distinguishing quartz and feldspar in single grain luminescence measurements. Radiation Measurements 37: 161-165.

Duller GAT (2007). Assessing the error on equivalent dose estimates derived from single aliquot regenerative dose measurements. Ancient TL 25: 15-24.

Erginal AE, Ekinci YL, Demirci A, Bozcu M, Ozturk MZ et al. (2013). First record of beachrock on Black Sea coast of Turkey: implications for Late Holocene sea-level fluctuations. Sedimentary Geology 294: 294-302.

Erol O (1952). Trabzon şekilleri hakkında bir not. Dil ve Tarih Coğrafya Fakültesi Dergisi 10: 125-136 (in Turkish).

Erturaç MK (2020). Late Pleistocene-Holocene characteristics of the North Anatolian Fault at Adapazarı Basin: evidences from the age and geometry of the fluvial terrace staircases. Turkish Journal of Earth Sciences 30: 93-115. doi: 10.3906/yer-2006-25

Erturaç MK, Güneç Kıyak N (2017). Yeşilırmak taraçalarında (Orta Kuzey Anadolu) geç pleyistosen iklim değişiklikleri ve düşey yönlü deformasyona akarsu cevabının araştırılması. Türkiye Jeoloji Bülteni 60: 615-636. doi: 10.25288/tjb.370625 (in Turkish).

Eyuboglu Y, Bektas O, Seren A, Nafız M, Jacoby WR et al. (2006). Three-directional extensional deformation and formation of the Liassic rift basins in the eastern Pontides (NE Turkey). Geologica Carpathica 57 (5): 337-346.

Eyuboglu Y, Bektaş O, Pul D (2007). Mid-Cretaceous olistostromal ophiolitic melange developed in the back-arc basin of the eastern Pontide magmatic arc (NE Turkey). International Geology Review 49 (12): 1103-1126.

Eyuboglu Y, Santosh M, Bektaş O, Ayhan S (2011). Arc magmatism as a window to plate kinematics and subduction polarity: example from the eastern Pontides belt, NE Turkey. Geoscience Frontiers 2 (1): 49-56.

Fattahi M, Walker R, Hollingsworth J, Bahroudi A, Nazari H et al. (2006). Holocene slip-rate on the Sabzevar thrust fault, NE Iran, determined using optically-stimulated luminescence (OSL). Earth Planetary Science Letter 245 (3-4): 673-684.

Fattahi M, Nazari H, Bateman MD, Meyere B, Sébrier M et al. (2010). Refining the OSL age of the last earthquake on the Dheshir fault, Central Iran. Quaternary Geochronology 5 (2-3): 286-292.

Florentin JA, Blackwell BAB, Tüysüz O, Tarı U, Genç ŞC et al. (2014). Monitoring tectonic uplift and paleoenvironmental reconstruction for marine terraces near Mağaracık and Samandağ, Hatay Province, Turkey. Radiation Protection Dosimetry 159 (1/4): 220-232. doi: 10.1093/rpd/ncu179

Galbraith RF (1990). The radial plot: graphical assessment of spread in ages. Nuclear Tracks and Radiation Measurements 17: 197-206.

Galbraith RF, Roberts RG, Laslett GM, Yoshida H, Olley JM (1999). Optical dating of single and multiple grains of quartz from Jinmium rock shelter, northern Australia: part I, experimental design and statistical models. Archaeometry 4: 339-364.

Galbraith RF, Roberts RG, Yoshida H (2005). Error variation in OSL palaeodose estimates from single aliquots of quartz: a factorial experiment. Radiation Measurements 39: 289-307.

Galbraith RF, Roberts RG (2012). Statistical aspects of equivalent dose and error calculation and display in OSL dating: an overview and some recommendations. Quaternary Geochronology 11: 1-27.

Gedikoğlu A (1970); Etude Géologique de la Région de Gölköy (Province D' Ordu-Turquie). PhD, University of Grenoble, Grenoble, France.

Gilmore GR (2008). Practical gamma-ray spectrometry. 2nd ed. Warrington, UK: John Wiley & Sons, Ltd.

Gök R, Mellors RJ, Sandvol E, Pasyanos M, Hauk T et al. (2016). Lithospheric velocity structure of the Anatolian plateau Caucasus-Caspian region. Journal of Geophysical Research Solid Earth 116 (B5): 2156-2202.

Gurrola LD, Keller EA, Chen JH, Owen LA, Spencer JQG (2014). Tectonic geomorphology of marine terraces: Santa Barbara fold belt, California. Geological Society of America Bulletin 126: 219-233.

Güven İH (1993). Geological and Metallogenic Map of the Eastern Black Sea Region; 1:250,000 Map. Trabzon, Turkey: General Directorate of Mineral Research and Exploration.

Grün R (1989). Electron spin resonance (ESR) dating. Quaternary International 1: 65-109.

Hamilton WJ (1842). Researches in asia minor, pontus and armenia with some account of their antiquities and geology. 1st ed. London, UK: Cambridge University Press.

Hässig M, Duretz T, Rolland Y, Sosson M (2016). Obduction of old oceanic lithosphere (80 Ma) due to thermal rejuvenation and the role of postobduction extension, insights from NE Anatolia-Lesser Caucasus ophiolite and numerical modelling. Journal of Geodynamics 96: 35-49.

Hiscott RN, Aksu AE, Yaşar D, Kaminski MA, Mudie PJ et al. (2002). Deltas south of the Bosphorus Strait record persistent Black Sea outflow to the Marmara Sea since ~10 ka. Marine Geology 190: 95-118.

Hiscott RN, Aksu AE, Mudie PJ, Kaminski MA, Abrajano T et al. (2007). The Marmara Sea gateway since ~16 ky BP: non-catastrophic causes of paleoceanographic events in the Black Sea at 8.4 and 7.15 ky BP. In: Yanko-Hombach V, Gilbert AS, Dolukhanov PM (editors). The Black Sea Flood Question. Netherlands: Springer, pp. 89-117.

Hreinsdóttir S, Bennett RA (2009). Active aseismic creep on the Alto Tiberina low-angle normal fault, Italy. Geology 27 (8): 683-686.

Jacobs Z (2008). Luminescence chronologies for coastal and marine sediments. Boreas 37: 508-535.

Jara-Muñoz J, Melnick D, Brill D, Strecker MR (2015). Segmentation of the 2010 Maule Chile earthquake rupture from a joint analysis of uplifted marine terraces and seismic cycle deformation patterns. Quaternary Science Review 113: 171-192. doi: 10.1016/j.quascirev.2015.01.005

Johnson WC, Halfen AF, Spencer JQG, Hanson PR, Mason JA et al. (2019). Late MIS 3 stabilization of dunes in the eastern Central Great Plains, USA. Aeolian Research 36: 68-81.

Karabacak V, Altunel E, Çakır Z (2011). Monitoring aseismic surface creep along the North Anatolian Fault (Turkey) using groundbased LIDAR. Earth and Planetary Science Letters 304 (1-2): 64-70.

Karajiyan H (1920). Mineral Resources of Armenia and Anatolia. 1st ed. Newyork, NY, USA: Armenia Press.

Keskin S (2007). Güneydoğu (GD) Karadeniz Sahil Kesiminin (Trabzon Yöresi) Denizel Taraçaları ve Aktif Tektoniği. Master Thesis, Karadeniz Technical University, Trabzon, Turkey (in Turkish).

Keskin S, Pedoja K, Bektas O (2011). Coastal uplift along the eastern Black Sea coast: new marine terrace data from Eastern Pontides, Trabzon (Turkey) and a Review. Journal of Coastal Research 27: 63-73.

Koçyiğit A, Yılmaz A, Adamia S, Kuloshvili S (2001). Neotectonics of East Anatolian Plateau (Turkey) and Lesser Caucasus: implication for transition from thrusting to strike-slip faulting. Geodinamica Acta 14: 177-95.

Krijgsman W, Tesakov A, Yanina T, Lazarev S, Danukalov G et al. (2019). Quaternary time scales for the Pontocaspian domain: Interbasinal connectivity and faunal evolution. Earth-Science Reviews 188:1-40. doi: 10.1016/j.earscirev.2018.10.013

Kurbanov RN, Svitoch AA, Yanina TA (2014). New Data on Marine Pleistocene Stratigraphy of the Western Cheleken Peninsula. Doklady Earth Sciences 459 (2): 1623-1626. doi: 10.1134/S1028334X14120265

Lajoie KR (1986). Coastal tectonics. In: Wallace RE (editor). Active Tectonics: Impact on Society. Washington, DC, USA: The National Academies Press, pp. 95-124.

Lamothe M (2016). Luminescence dating of interglacial coastal depositional systems: Recent developments and future avenues of research. Quaternary Science Reviews 146: 1-27.

Maden N, Özturk S (2015). Seismic b-values, bouguer gravity and heat flow data beneath Eastern Anatolia, Turkey: Tectonic implications. Surveys in Geophysics 36: 549-570.

McClusky S, Balassanian S, Barka A, Demir C, Ergintav S et al. (2000). Global Positioning System constraints on plate kinematics and dynamics in the eastern Mediterranean and Caucasus. Journal of Geophysical Research B Solid Earth 105: 5695-5719.

McClusky S, Reilinger R, Mahmoud S, Ben Sari D, Tealeb A (2003). GPS constraints on Africa (Nubia) and Arabia plate motion: Geophysical Journal International 155: 126-138.

McKenzie D (1972). Active tectonic of the Mediterranean region. Geophysical Journal of the Royal Astronomical Society 30: 109-185.

Murray AS, Wintle AG (2000). Luminescence dating of quartz using an improved single aliquot regenerative-dose protocol. Radiation Measurements 33: 57-73.

Murray AS, Wintle AG (2003). The single aliquot regenerative dose protocol: potential for improvements in reliability. Radiation Measurements 37: 377-381.

Murray AS, Marten R, Johnston A, Martin P (1987). Analysis for naturally occurring radionuclides at environmental concentrations by gamma spectrometry. Journal of Radioanalytical and Nuclear Chemistry 115: 263-288.

Nalin R, Lamothe M, Auclair M, Massari F (2020). Chronology of the marine terraces of the Crotone Peninsula (Calabria, southern Italy) by means of infrared-stimulated luminescence (IRSL). Marine and Petroleum Geology 122: 104645.

Nas M, Lyubushin A, Softa M, Bayrak Y (2020). Comparative PGA-driven probabilistic seismic hazard assessment (PSHA) of Turkey with a Bayesian perspective. Journal of Seismology. doi: 10.1007/s10950-020-09940-5

Nesmeyanov SA. (1995). Pleistocene deformation of Black Sea terraces along the Caucasus coast. Geotectonics 29 (3): 259-269.

Nilforoushan F, Masson F, Vernant P, Vigny C, Martinod J et al. (2003). GPS network monitors the Arabia-Eurasia collision deformation in Iran. Journal of Geodesy 77: 411-422.

Normand R, Simpson G, Herman F, Biswas RH, Bahroudi A et al. (2019). Dating and morpho-stratigraphy of uplifted marine terraces in the Makran subduction zone (Iran). Earth Surface Dynamics 7 (1): 321-344.

Okay A, Zattin M, Sunal G (2020). Uplift of Anatolia. Turkish Journal of Earth Sciences 29: 696-713.

Ortlieb L, Fournier M, Macharé J (1992). Sequences of Holocene beach ridges in northern Peru–chronological framework and possible relationships with former El Niño events. In: Paleo ENSO Records International Symposium; Lima, Peru. pp. 215-223.

Oswald F (1906). Geology of Armenia. PhD, University of London, London, UK.

Özalp S (2020). Late Pleistocene-Holocene lake terraces, water level change, and active tectonics: Eastern coast of Lake Van, Eastern Anatolia, Turkey. Quaternary International 542: 54-64. doi: 10.1016/j.quaint.2020.02.037

Özkaymak C, Sozbilir H, Gecievi OM, Tiryakioglu I (2019). Late Holocene coseismic rupture and aseismic creep on the Bolvadin Fault, Afyon Akşehir Graben, Western Anatolia. Turkish Journal of Earth Sciences 28: 787-804.

Özsayar T (1971). Palaontologie und Geologie des Gebietes Ostlich Trabzon (Anatolien). PhD Thesis, University of Giessen, Germany.

Panin N (1983). Black Sea Coast line changes in the Last 10.000 Years. A new attempt at identifying the Danube mouths as described by the ancients. Dacia. Revue d'Archéologie et d'Histoire Ancienne Bucuresti 27 (1-2): 175-184.

Panin N, Popescu I (2007). The northwestern Black Sea: climatic and sea-level changes in the late Quaternary. In: Yanko-Hombach Y, Gilbert AS, Panin N, Dolukhanov P. (Eds). The Black Sea Flood Question: Changes in Coastline, Climate, and Human Settlement. Dordrecht, The Netherlands: Springer, pp. 387-404.

Pedoja K, Dumont JF, Lamothe M, Ortlieb L, Collot JY et al. (2006). Plio-Quaternary uplift of the Manta Peninsula and La Plata Island and the subduction of the Carnegie Ridge, central coast of Ecuador. Journal of South American Earth Sciences 22:1-21. doi: 10.1016/j.jsames.2006.08.003

Pedoja K, Husson L, Regard V, Cobbold PR, Ostanciaux E et al. (2011). Relative sea-level fall since the last interglacial stage: are coasts uplifting worldwide? Earth Science Review 108 (1-2): 1-15.

Pedoja K, Husson L, Bezos A, Pastier A, Imran AM et al. (2018). On the long-lasting sequences of coral reef terraces from SE Sulawesi (Indonesia): distribution, formation, and global significance. Quaternary Science Review 188: 37-57. doi: 10.1016/j.quascirev.2018.03.033

Philip H, Cisternas A, Gvishiani A, Gorshkov A (1989). The Caucasus: an actual example of the initial stage of continental collision. Tectonophysics 161: 1-21.

Preusser F, Degering D, Fuchs M, Hilgers A, Kadereit A et al. (2008). Luminescence dating: basics, methods and applications. Quaternary Science Journal 57 (1-2): 95-149.

Prescott JR, Hutton JT (1994). Cosmic ray contributions to dose rates for luminescence and ESR dating: Large depths and long-term time variations. Radiation Measurements 23: 497-500. doi: 10.1016/1350-4487(94)90086-8

Railsback LB, Gibbard PL, Head MJ, Voarintsoa NRG, Toucanne S (2015). An optimized scheme of lettered marine isotope substages for the last 1.0 million years, and the climatostratigraphic nature of isotope stages and substages. Quaternary Science Reviews 111: 94-106. doi: 10.1016/j.quascirev.2015.01.012

Rhodes EJ, Singarayer JS, Raynal JP, Westaway KE, Sbihi-Alaoui FZ (2006). New age estimates for the Palaeolithic assemblages and Pleistocene succession of Casablanca, Morocco. Quaternary Science Reviews 25: 2569-2585.

Rhodes EJ (2011). Optically Stimulated Luminescence Dating of Sediments over the Past 200,000 Years. Annual Review of Earth and Planetary Sciences 39: 461-488.

Riedel W (1929). Zur mechanik geologischer brucherscheinungen. Zentralblatt für Mineralogie. Geologie Und Paläontologie 1929 (B): 354-368.

Roberts RG, Galbraith RF, Olley JM, Yoshida H, Laslet GM (1999). Optical dating of single and multiple grains of quartz from Jinmium Rock Shelter, Northern Australia: Part II, results and implication. Archaeometry 41: 365-395.

Roberts GP, Meschis M, Houghton S, Underwood C, Briant RM (2013). The implications of revised Quaternary paleo shoreline chronologies for the rates of active extension and uplift in the upper plate of subduction zones, Quaternary Science Review 78: 169-187. doi: 10.1016/j.quascirev.2013.08.006

Ryan WBF, Major CO, Lericolais G, Goldstein SL (2003). Catastrophic flooding of the Black Sea. Annual Review of Earth and Planetary Sciences 31: 525-554.

Ryan WBF (2007). Status of the Black Sea flood hypothesis. In: Yanko-Hombach V, Gilbert AS, Dolukhanov PM (editors). The Black Sea Flood Question. The Netherlands: Springer, pp. 63-88.

Saillard M, Hall SR, Audin L, Farber DL, Hérail G et al (2009). Non-steady long-term uplift rates and Pleistocene marine terrace development along the Andean margin of Chile (31S) inferred from 10Be dating. Earth Planetary Science Letters 277: 50-63. doi: 10.1016/j.epsl.2008.09.039

Sançar T, Zabcı C, Akçar N, Karabacak V, Yeşilyurt S et al (2020). Geodynamic importance of the strike-slip faults at the eastern part of the Anatolian Scholle: Inferences from the uplift and slip rate of the Malatya Fault (Malatya-Ovacık Fault Zone, eastern Turkey). Journal of Asian earth sciences 188: 104091.

Schulz SS, Mavko GM, Burford RO, Stuart WD (1982). Long-term fault creep observations in central California, Journal Geophysical Research 87: 6977-6982.

Schwarcz HP (1989). Uranium series dating of Quaternary deposits. Quaternary International 1: 7-17.

Semerci A (1990). Trabzon Ili Yerlesim Alaninin Muhendislik Jeolojisi Acisindan Incelenmesi. Master Thesis, Karadeniz Technical University, Trabzon, Turkey (in Turkish).

Siddall M, Chappell J, Potter EK (2006). Eustatic Sea level during past interglacials. In: Sirocko F, Litt T, Claussen M, Sanchez-Goni MF (editors). The Climate of Past Interglacials. Amsterdam, Netherlands: Elsevier, pp. 75-92.

Sieh KE, Williams PH (1990). Behavior of the southernmost San Andreas Fault during the past 300 years. Journal of Geophysical Research 95 (B5): 6629-6645.

Smith AD, Taymaz T, Oktay F, Yüce H, Alpar B et al. (1995). High resolution seismic reflection profiling in the Sea of Marmara (northwest Turkey): late Quaternary sedimentation and sea-level changes. Bulletin of the Geological Society of America 107: 923-936.

Softa M, Emre T, Sözbilir H, Spencer JQG, Turan M (2018). Geomorphic evidence for active tectonic deformation in the coastal part of Eastern Black Sea, Eastern Pontides, Turkey. Geodinamica Acta 30 (1): 249-264.

Softa M, Emre T, Sözbilir H, Spencer JQG, Turan M (2019). Field evidence for Southeast Black Sea Fault of Quaternary age and its tectonic implications, Eastern Pontides, Turkey. Geological Bulletin of Turkey 62: 17-40.

Solmaz F (1990). Vakfikebir-Yomra arası kıyı şeridinin morfolojisi ve taraçalar. Master Thesis, İstanbul University, İstanbul, Turkey (in Turkish).

Sosson M, Stephenson R, Sheremet Y, Rolland Y, Adamia S et al. (2016). The Eastern Black Sea-Caucasus region during the Cretaceous: new evidence to constrain its tectonic evolution. Comptes Rendus Geoscience 348: 23-32.

Spencer JQG, Oviatt CG, Pathak M, Fan Y (2015). Testing and refining the timing of hydrologic evolution during the latest Pleistocene regressive phase of Lake Bonneville. Quaternary International 362: 139-145.

Spencer JQG, Robinson RAJ (2008). Dating intramontane alluvial deposits from NW Argentina using luminescence techniques: problems and potential. Geomorphology 93: 144-156.

Spratt RM, Lisiecki LE (2016). A Late Pleistocene sea level stack. Climate of the Past 12:1079-1092. doi: 10.5194/cp-12-1079-2016

Stahl T, Quigley MC, McGill A, Bebbington MS (2016). Modeling earthquake moment magnitudes on imbricate reverse faults from paleoseismic data: Fox Peak and Forest Creek Faults, South Island, New Zealand. Bulletin Seismological Society of America 106 (5): 2345-2363.

Şengör AMC (1979). The North Anatolian transform fault: its age, offset and tectonic significance. Journal of Geological Society 136: 269-282.

Şengör AMC, Yılmaz Y (1981). Tethyan evolution of Turkey: a plate tectonic approach. Tectonophysics 75: 181-241.

Tanaka K, Hataya R, Spooner NA, Questiaux DG, Saito Y et al. (1997). Dating of marine terrace sediments by ESR, TL and OSL methods and their applicabilities. Quaternary Science Reviews 16: 257-264.

Tarı U, Tüysüz O, Blackwell BAB, Mahmudd Z, Florentin JA et al (2018). Sea level change and tectonic uplift from dated marine terraces along the eastern Mediterranean coast, southeastern Turkey. Palaeogeography, Palaeoclimatology, Palaeoecology 511 (15): 80-102. doi: 10.1016/j.palaeo.2018.07.003

Tsereteli N, Tibaldi A, Alania V, Gventsadse A, Enukidze O et al. (2016). Active tectonics of central-western Caucasus, Georgia. Tectonophysics 691: 328-344.

Tsodoulos IM, Stamoulis K, Caputo R, Koukouvelas I, Chatzipetros A et al. (2016). Middle-Late Holocene earthquake history of the Gyrtoni Fault, Central Greece: insight from optically stimulated luminescence (OSL) dating and paleoseismology. Tectonophysics 687: 14-27.

Urbanova P, Hourcade D, Ney C, Guibert P (2015). Sourecs of uncertainties in OSL dating of archaeological mortars: the case study of the Roman amphitheatre "Palais-Gallien" in Bordeaux. Radiation Measurements 72: 100-110.

Ustaömer T, Robertson AHF (1996). Paleotethyan tectonic evolution of the north Tethyan margin in the central Pontides, N Turkey. In: Erler A, Ercan T, Bingol E, Orcen S. (editors). Proceedings of the International Symposium on the Geology of the Black Sea Region. Ankara, Turkey: General Directorate of Mineral Reasearch and Exploration and Chamber of Geological Engineers, pp. 24-33.

Vialon P, Ruhland M, Grolier J (1976). Eléments de tectonique analytique. 1 st ed. Paris, France: Masson.

Westaway R (1994). Present-day kinematics of the Middle East and eastern Mediterranean. Journal of Geophysical Research 99: 12071-12090.

Wilcox RE, Harding TP, Seely DR (1973). Basic wrench tectonics. AAPG Bulletins 57: 74-96.

Wintle AG, Murray AS (2006). A review of quartz optically stimulated luminescence characteristics and their relevance in single-aliquot regeneration dating protocols. Radiation Measurements 41: 369-391.

Yaltırak C, Sakınç M, Aksu AE, Hiscott RN, Galleb B et al. (2002). Late Pleistocene uplift history along the southwestern Marmara Sea determined from raised coastal deposits and global sea-level variation. Marine Geology 190: 283-305.

Yanchilina AG, Ryan WBF, McManus JF, Dimitrov P, Dimitrov D et al (2017). Compilation of geophysical, geochronological, and geochemical evidence indicates a rapid Mediterranean-derived submergence of the Black Sea's shelf and subsequent substantial salinification in the early Holocene. Marine Geology 383: 14-34.

Yanina TA (2012). Correlation of the Late Pleistocene paleogeographical events of the Caspian Sea and Russian Plain. Quaternary International 271: 120-129. doi: 10.1016/j.quaint.2012.06.003

Yanina TA (2013). Biostratigraphy of the middle and upper Pleistocene of the Caspian region. Quaternary International 284: 85-97.

Yanina TA (2014). The Ponto-Caspian region: environmental consequences of climate change during the Late Pleistocene. Quaternary International 345: 88-99.

Yanko-Hombach V, Gilbert AS, Panin N, Dolukhanov PM (2007). The Black Sea Flood Question: Changes in Coastline, Climate and Human Settlement. New York, NY, USA: Springer.

Yildirim C, Schildgen TF, Echtler H, Melnick D, Strecker MR (2011). Late Neogene and active orogenic uplift in the Central Pontides associated with the North Anatolian Fault: implications for the northern margin of the Central Anatolian Plateau, Turkey. Tectonics 30: TC5005.

Yildirim C, Melnick D, Ballato P, Schildgen TF, Echtler H et al. (2013). Diferential uplift along the northern margin of the Central Anatolian Plateau: inferences from marine terraces. Quaternary Science Reviews 81: 12-28.

Yılmaz Y, Tüysüz O, Yiğitbaş E, Genç ŞC, Şengör AMC (1997). Geology and tectonic evolution of the Pontides, In: Robinson AG (editor). Regional and Petroleum Geology of the Black Sea and Surrounding Regions (AAPG Memoir 68). Tulsa, OK, USA: The American Association of Petroleum Geologists, pp. 183-226.

Yilmaz BS, Guc AR, Gulibrahimoglu I, Yazici EN, Konak O et al. (1998). Trabzon İlinin Çevre Jeolojisi ve Doğal Kaynakları. Ankara, Turkey: Maden Tetkik ve Arama Genel Müdürlüğü (in Turkish).

Yilmaz C, Sen C, Sener S, Kandemir R, Karsli O et al. (2005). Trabzon Kiyi Bolgesinin Pliyo-Kuvaterner Stratigrafisi. In: Quaternary Symposium of Turkey; İstanbul, Turkey. pp. 111-117 (in Turkish).

Zastrozhnov A, Danukalova G, Golovachev M, Titov V, Osipova E et al (2020). Biostratigraphical investigations as a tool for palaeoenvironmental reconstruction of the Neopleistocene (Middle-Upper Pleistocene) at Kosika, Lower Volga, Russia. Quaternary International 540: 38-67. doi: 10.1016/j.quaint.2018.11.036

Zimmerman DW (1971). Thermoluminescent dating using fine grains from pottery. Archaeometry 13: 29-52. doi: 10.1111/j.1475-4754.1971.tb00028.x

Zubakov VA, Kochegura VV (1974). The Late Pliocene and Quaternary. In: Zubakov VA (editor). Geochronology of the USSR. Vol 3. Leningrad, Russia: Nedra Publishers (in Russian).

Zubakov VA (1988). Climatostratigraphic scheme of the Black Sea Pleistocene and its correlation with the oxygen-isotope scale and glacial event. Quaternary Research 29:1-24.